Science of Advanced Materials
Vol. 3, 80–88, 2011

Structural, Compositional and Magnetic Studies on $Zn_{1-x}Cr_xTe$ ($x = 0.05, 0.15$) Films Grown on GaAs (100) Substrates

D. Soundararajan[1,7], D. Mangalaraj[2,*], D. Nataraj[1], L. Dorosinskii[3], J. Santoyo-Salazar[4,5], K. Senthil[6], and J. M. Ko[7,*]

[1] *Thin Films & Nanomaterials Lab, Department of Physics, Bharathiar University, Coimbatore 641046, India*
[2] *Department of Nanoscience & Technology, Bharathiar University, Coimbatore 641046, India*
[3] *National Institute of Metrology (TUBITAK - UME), P.K. 54, 41470, Gebze, Kocaeli, Turkey*
[4] *Universidad Nacional Autonoma de Mexico, Instituto de Investigaciones en Materiales, Mexico D.F. AP 70-360, 04510, Mexico*
[5] *Institut de Physique et Chimie des Matériaux de Strasbourg, UMR CNRS-ULP-ECPM 7504, 23, rue du Loess, BP 43, 67034 Strasbourg cedex, France*
[6] *Center for Information Materials, Pohang University of Science and Technology (POSTECH), Pohang 790-784, South Korea*
[7] *Division of Applied Chemistry & Biotechnology, Hanbat National University, San 16-1, Dukmyung-Dong, Yusung-Gu, Daejeon 305-719, South Korea*

ZnTe and Cr doped ZnTe films were prepared by using a thermal evaporation method. $Zn_{1-x}Cr_xTe$ ($x = 0.0$, 0.05, 0.15) films were grown on GaAs (100) substrates at ambient temperature. X-ray diffraction (XRD) measurements showed the presence of ZnCrTe phase with a minute amorphous background, which slightly increased with the Cr concentration. Compositional analyses by X-ray Photoemission Spectroscopy (XPS) disclosed the presence of antiferromagnetic Cr_2O_3 and Cr precipitates. From the XPS and Electron Spin Resonance (ESR) spectra analysis, the valence state of Cr in ZnTe was found to be +2 with d^4 electronic configuration. Magnetic Force Microscopy (MFM) analysis showed the presence of domains with an average size of 1–2 nm. Magnetic properties, such as magnetic moment versus magnetic field dependence, were recorded with Superconducting Quantum Interference Device (SQUID) magnetometry at 300 K. The data obtained reveal the persistence of ferromagnetic behavior at 300 K. From the Arrott plot analysis, the Curie temperature was estimated to be much greater than 300 K.

Keywords: Dilute Magnetic Semiconductor, ZnTe:Cr Film, Magnetic Studies.

1. INTRODUCTION

Semiconductors doped with transition metal impurities, called diluted magnetic semiconductors (DMSs), are important in modern semiconductor spintronics. In conventional metal-based spintronics, ferromagnetic (FM) metals are used as spin current injection/magnetic storage layers. One advantage offered by DMSs over FM metals is the smaller lattice mismatch that its semiconductor partner would experience in heterojunction structures, unlike the case of a FM layer. This makes research on DMSs an actively tacked area due to the technological potential for use in spintronic devices and their interesting magnetic and transport properties.[1–7]

The main requirement that a DMS should meet is that it should exhibit ferromagnetic behavior above room temperature, without any secondary phase being involved. The discovery of ferromagnetism in (In, Mn)As[3] and (Ga, Mn)As[4] promoted DMSs as fundamental materials for spintronics because of their compatibility with semiconductors used in present electronics. However, the Curie temperature (T_C) of DMSs may not be high enough for practical applications. Besides III–V compound semiconductors, II–VI compound semiconductors have also been used as DMSs upon doping with transition metal (TM) impurities, such as Fe, Mn and Co. This approach does not provide ferromagnetic behavior, but confers spin glass or antiferromagnetic properties to II–VI compound semiconductors.[8]

*Authors to whom correspondence should be addressed.

 1947-2935/2011/3/080/009 doi:10.1166/sam.2011.1134

However, it has recently been reported that highly p-doped ZnTe:Mn film can show ferromagnetism at the temperature of 300 K.[9] This is due to the mediation of the ferromagnetic ordering among magnetic ions by the added hole carriers.[10] On the contrary, it has been predicted that when TM impurities, such as Cr, are doped into a II–VI compound semiconductors, such as ZnTe, net ferromagnetic exchange interactions should result in even without *p*- or *n*-type doping.[11] The reason is that in the case of Cr-doping into II–VI semiconductors, replacement of cation (Zn) positions itself acts as a source of holes as well as a source of magnetic impurities. This is unlike the case of Fe- or Mn-doping into II–VI semiconductors, where a separate hole dopant is also required in addition to the magnetic impurity dopants (Fe, Co, and Mn).[12] Room-temperature ferromagnetic behavior was observed when Cr was heavily doped into ZnTe films and (Zn,Cr)Te was proved to be a real DMS. Saito et al. reported experimentally that $Zn_{1-x}Cr_xTe$ sample with $x = 0.2$, exhibited ferromagnetism at room temperature.[13, 14]

In general, ZnTe:Cr films were prepared by Molecular Beam Epitaxy (MBE) technique by many researchers.[13–16] In our earlier report, we presented magnetic[17] and magneto-optical[18] studies on ZnTe:Cr films on glass prepared by using a thermal evaporation method. In the present investigation, we illustrate a detailed study on the structural, compositional and magnetic properties of vacuum-evaporated $Zn_{1-x}Cr_xTe$ ($x = 0.05, 0.15$) films grown onto GaAs (100).

2. EXPERIMENTAL DETAILS

Film deposition. Appropriate amounts of high-purity Zn, Te and Cr (Alfa Aeser) metals were taken weighted together inside three separate quartz ampoules for the preparation of $Zn_{1-x}Cr_xTe$ alloys with $x = 0.0$, 0.05 and 0.15. In case of pure ZnTe, the vacuum-sealed ampoule was maintained at 600 °C for 12 h. In the case of ZnTe:Cr, the ampoules were maintained at 1100 °C for 24 h. In both cases, the temperature of the furnace was slowly increased step-by-step to the set value. After the reaction had been carried out for suitable time period, the temperature was slowly decreased in steps to room temperature. The molten alloy was taken out and made into fine powder by grinding in a mortar and then used for the growth of films. The $Zn_{1-x}Cr_xTe$ compound powder with $x = 0.0$, 0.05, and 0.15 were thermally evaporated from a tungsten dimple source onto well-cleaned GaAs (100) substrates under a vacuum of 4×10^{-5} torr at ambient temperature. The growth of each $Zn_{1-x}Cr_xTe$ film with $x = 0.0$, 0.05, 0.15 were performed individually.

Characterization techniques. In order to determine the crystal structure of $Zn_{1-x}Cr_xTe$ ($x = 0.0$, 0.05, 0.15) films grown on GaAs (100) substrate, X-ray Diffraction (XRD) patterns were recorded in the 2θ scan range of 20° to 80° by using a X-ray diffractometer (Model - Shimadzu (XRD-6000), $\lambda = 1.5406$ Å). X-ray Photoemission Spectroscopy (XPS) measurements were carried out using an Escalab 220iXL system (VG Scientific Inc.) with a monochromatic Mg Kα X-ray source (1284.6 eV). The ultimate XPS determination accuracy was of about 0.1 atomic percentages. First-derivative absorption electron spin resonance (ESR) spectra were recorded by using an E-112 Varian ESR Spectrometer at X-band frequency at 75 K. *Ex-situ* topography and magnetic domain pattern studies were performed by means of Scanning Probe Microscope (SPM) (JEOL JSPM-4210). The particle size and magnetic domains were scanned in room temperature conditions. The topography of the films was scanned by Atomic Force Microscopy (AFM) microscope in Tapping™ mode, while magnetic domains were analyzed by Magnetic Force Microscopy (MFM) microscope in lift mode with magnetic cantilever tip NSC14/Co–Cr, Mikro-masch, Co. in resonant frequency of 160 kHz conditions. Magnetic domains were observed with lift interaction height of 25 nm and with an output of 0.025 amp/V. Measurements of two- (2D) and three-dimensional (3D) images, profiles, and domains were processed with the win SPM DPS, JEOL Ltd. Software. Magnetic data was collected by using a commercial SQUID magnetometer (Quantum Design MPMS—XL Superconducting Magnet) at 300 K.

3. RESULTS AND DISCUSSION

3.1. XRD Analysis

The XRD patterns of the source materials [$Zn_{1-x}Cr_xTe$ alloys with $x = 0.05$, 0.15] were compared with those of ZnTe to check their crystalline quality, as shown in Figure 1. As can be seen, the (111), (200), (220), (311), (222) and (400) reflections were observed to fit very well with those reported for the bulk cubic ZnTe lattice and the JCPDS data.[19] It was evident that a significant shift in the pattern of the doped samples was detectable in comparison with that of the undoped ZnTe sample. A shift in the diffraction peaks towards the lower angle side was commonly observed for powder samples with $x = 0.05$ and $x = 0.15$. This shift was larger for the heavily Cr-doped sample than for the lightly doped one. At such Cr concentrations, it was therefore expected that a significant change in the lattice parameter could be induced and the diffraction pattern of the undoped and doped samples should not be identical. This indicated that Cr was well incorporated into the ZnTe system. Further, additional reflections, such as the (103) and (102) that distinguished the ZnTe/ZnCrTe hexagonal phase,[19] were noticed for $Zn_{1-x}Cr_xTe$ with $x = 0.15$. This showed the coexistence of minute ZnTe/ZnCrTe hexagonal phase along with the dominant ZnTe/ZnCrTe cubic phase when Cr was heavily doped into ZnTe. This was unlike the case of alloys with low Cr content ($x = 0.05$), where only a pure ZnTe/ZnCrTe cubic zincblende phase was observed.

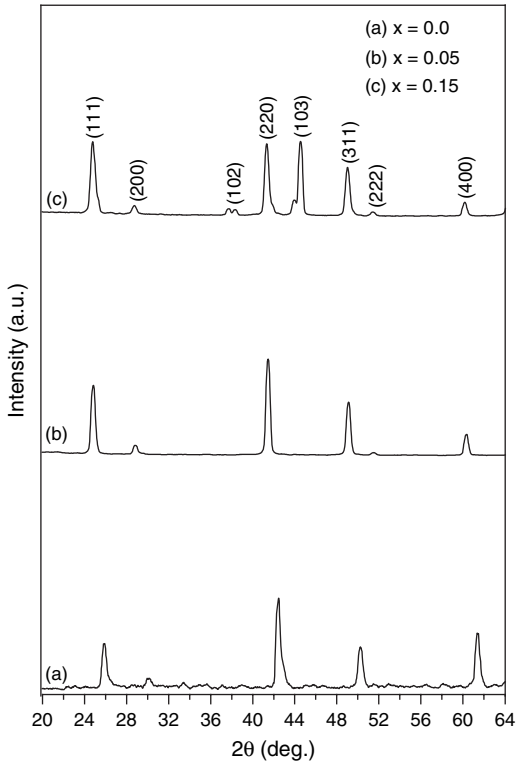

Fig. 1. XRD patterns of $Zn_{1-x}Cr_xTe$ alloy powder with (a) $x = 0.0$ (b) $x = 0.05$ and (c) $x = 0.15$.

Figure 2 shows the XRD patterns of $Zn_{1-x}Cr_xTe$ ($x =$ 0.0, 0.05, 0.15) films grown on GaAs (100). The result showed the presence of a diluted phase of cubic zincblende ZnCrTe and/or ZnTe along (111) and (400) reflections. Other reflections, such as the (200), (220), (311) and (222) that characterize the cubic zinc blende phase, were absent. Similar results were obtained by Kuroda et al., for the ZnCrTe films on GaAs (100) prepared by the MBE technique.[20] Upon comparing the diffraction patterns

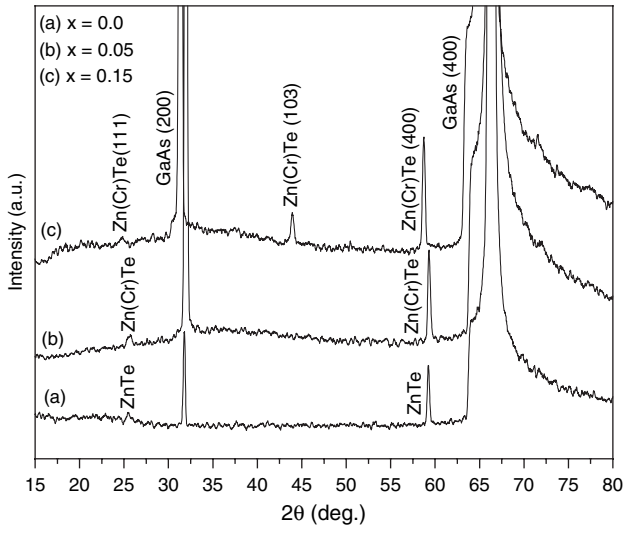

Fig. 2. XRD patterns of $Zn_{1-x}Cr_xTe$ films with (a) $x = 0.0$ (b) $x = 0.05$ and (c) $x = 0.15$ grown onto GaAs (100) substrate.

of films with $x = 0.05$ and 0.15, an additional reflection (103) that characterize ZnTe/ZnCrTe hexagonal phase was observed for heavily Cr-doped film with $x = 0.15$. This reflection was similarly observed in the diffraction pattern of its source material. In addition, a tiny amorphous shoulder along with the crystalline peaks was noticed in the 2θ scan range of 20° – 46° for films with $x = 0.05$ and 0.15. This amorphous shoulder was noticed to increase with increases in the Cr concentration. This indicated that the crystallinity of the film with $x = 0.15$ was relatively poorer than that of the film with $x = 0.05$.

3.2. XPS Study

The microscopic surface composition of the prepared $Zn_{1-x}Cr_xTe$ ($x = 0.0$, 0.05, 0.15) films was investigated by high-resolution XPS. Figures 3–5 show the XPS spectra of films with $x = 0.0$, 0.05 and 0.15, respectively. The

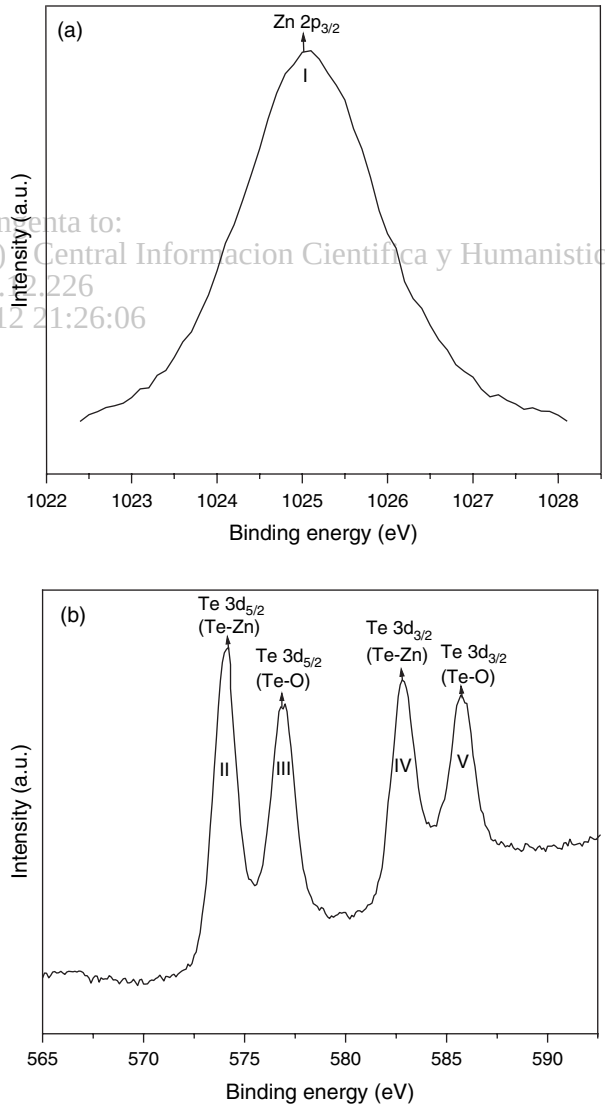

Fig. 3. High-resolution surface XPS spectra of ZnTe film.

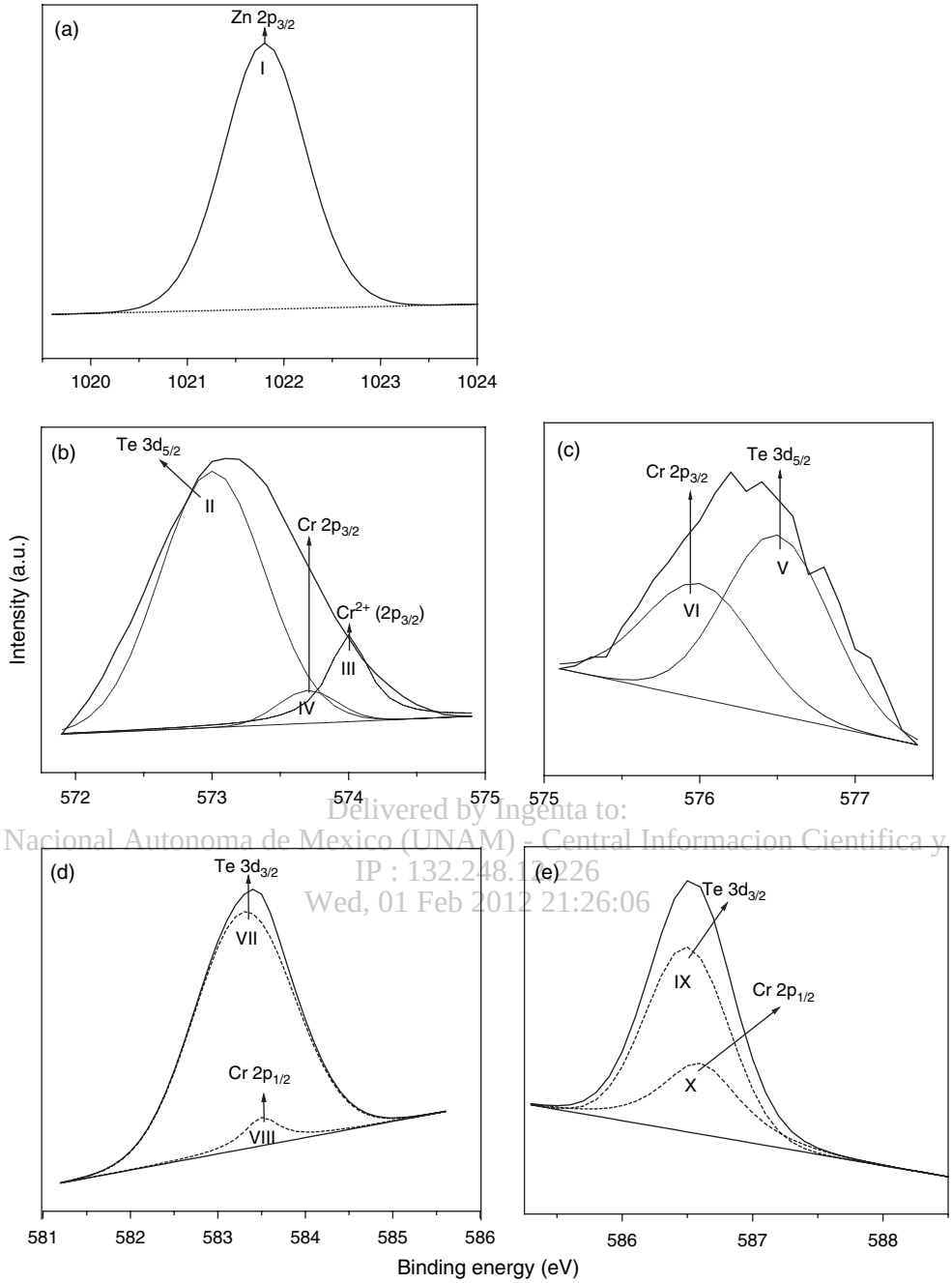

Fig. 4. High-resolution deconvoluted surface XPS spectra of a $Zn_{1-x}Cr_xTe$ film with $x = 0.05$.

most probable assignments to the origin of components in ZnTe and ZnTe:Cr films are presented in Tables I and II, respectively.[21] In the case of ZnTe, there appeared a single peak for Zn at 1025.08 eV, corresponding to a $2p_{3/2}$ transition. As for Te, two peaks appeared at 574.2 and 582.9 eV, corresponding to $3d_{5/2}$ and $3d_{3/2}$ transitions, respectively. In addition, adjacent to these two peaks another set of peaks was observable at 576.9 and 585.7 eV, again corresponding to $3d_{5/2}$ and $3d_{3/2}$ transitions in the oxidized phase of Te (TeO_2). The spectra relative to $Zn_{1-x}Cr_xTe$ ($x = 0.05$ and 0.15) films were deconvoluted because the core level binding energy of Cr and Te are close to each other. The presence of Cr^{2+} in the ferromagnetic Zn(Cr)Te/(Cr)Te phase was noticed at its corresponding binding energy of 574 eV.[21,22] In addition, the peaks at 576 eV and 573.7 eV indicated the presence of Cr_2O_3 and Cr, respectively.[22,23] These results pointed to the presence of secondary phases, such as Cr and Cr_2O_3, which are antiferromagnetic in nature.[24,25] A blue shift in the binding energy value of oxide related peaks suggested that Te/Cr had donated electrons to oxygen and therefore the binding energy corresponding to $3d$ and $3p$ transitions had

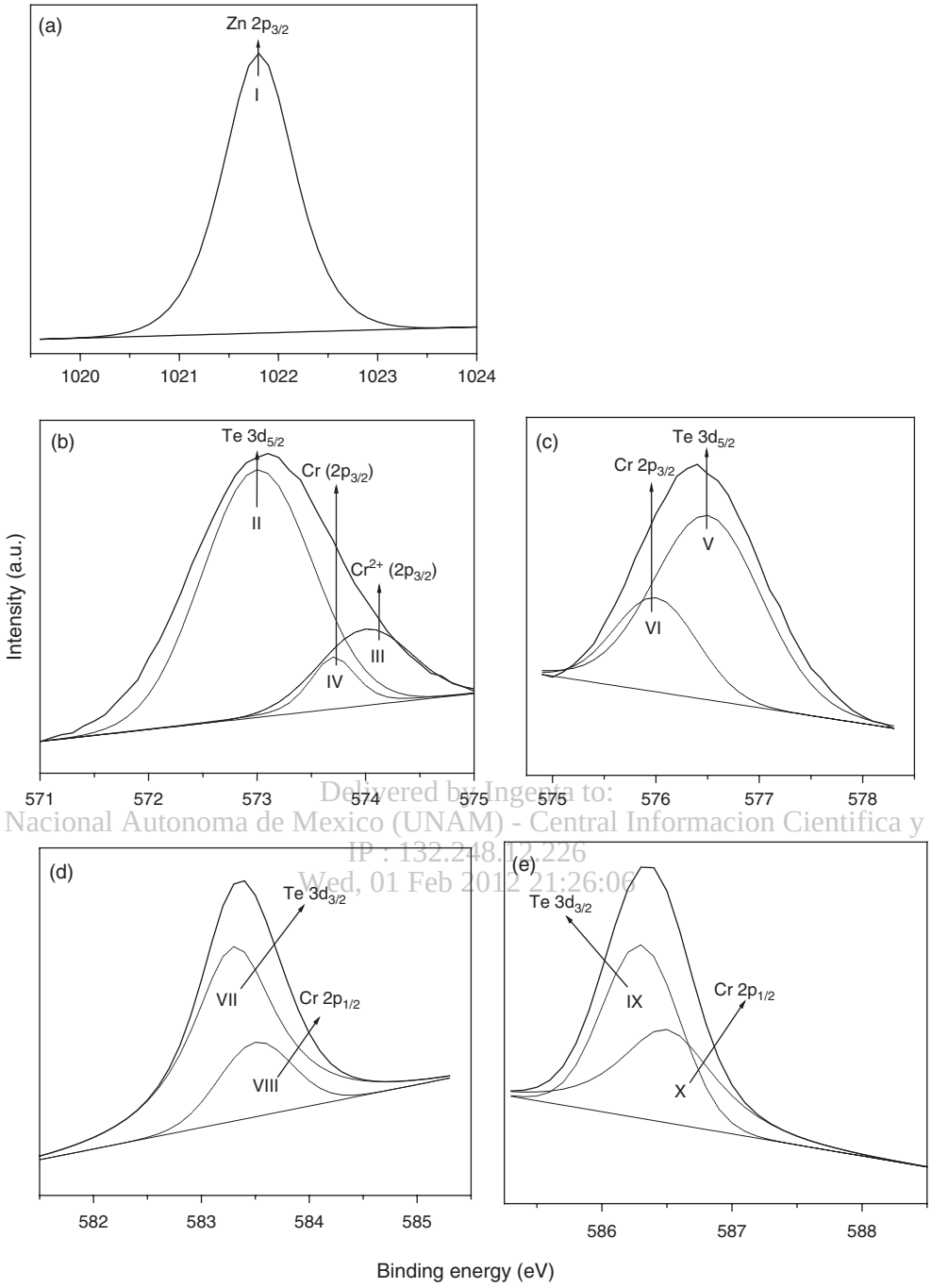

Fig. 5. High-resolution deconvoluted surface XPS spectra of a $Zn_{1-x}Cr_xTe$ film with $x = 0.15$.

increased. The stoichiometry of ZnTe and ZnTe:Cr films were determined by using the $2p$ peak for Zn, $3d$ peaks for Te and $2p$ peaks for Cr. The estimated values of relative atomic percentage of Zn, Te and Cr are given in Table III.

3.3. ESR Spectra

The advantage of ESR spectroscopy is its great sensitivity to the microscopic environment of the paramagnetic centre and is a tool to assess the valence state of Cr in the film. Therefore, the origin of magnetic moment from ZnTe:Cr film can be inferred. The electronic configuration of free Cr atom is $1s^2\ 2s^2\ 2p^6\ 3s^2\ 3p^6\ 3d^5\ 4s^1$. Chromium enters the ZnTe lattice substitutionally for the divalent cation and is expected to be in the Cr^{2+} valence state. ESR spectra of $Zn_{1-x}Cr_xTe$ films for $x = 0.05$ and $x = 0.15$ were recorded at 75 K and the obtained data is presented in Figure 6. Two signals were observed along with unresolved minute signals for both films. These two signals are marked as "1" and "2" in the spectra. The intensity of tiny peaks is

Table I. Assignments to the component peaks of the high-resolution surface XPS scans of the $Zn_{1-x}Cr_xTe$ film with $x = 0$.

Component	Binding energy (eV)	Assignment
I (Zn $2p_{3/2}$)	1025.08	Zn–Te
II (Te $3d_{5/2}$)	574.2	Te–Zn
IV (Te $3d_{5/2}$)	576.9	Te–O_2
VI (Te $3d_{3/2}$)	582.9	Te–Zn
VIII (Te $3d_{3/2}$)	585.7	Te–O_2

Table II. Assignments to the component peaks of the high resolution surface XPS scans of the $Zn_{1-x}Cr_xTe$ films with $x = 0.05$ and $x = 0.15$.

Component	Binding energy (eV)	Assignment
I (Zn $2p_{3/2}$)	1021.8	Zn–Te
II (Te $3d_{5/2}$)	573	Te–Zn
III (Cr $2p_{3/2}$)	574	Cr–Te
IV (Cr $2p_{3/2}$)	573.7	Cr–Cr
V (Te $3d_{5/2}$)	576.5	Te–O_2
VI (Cr$2p_{3/2}$)	575.6	Cr_2–O_3
VII (Te $3d_{3/2}$)	583.3	Te–Zn
VIII (Cr $2p_{1/2}$)	583.5	Cr–Te
IX (Te $3d_{3/2}$)	586.5	Te–O_2
X (Cr $2p_{1/2}$)	586.6	Cr_2–O_3

small, compared with signals "1" and "2". Hence, three electronic transitions should be allowed, and the total spin (S) should be 1, i.e., the Cr ion will have two unpaired electrons with $S = 1$ (since $2S + 1 = 3$). This fact indicated Cr with d^4 electronic configuration. Therefore, the signals are assigned to isolated Cr^{2+} ions substitutionally incorporated into the zinc lattice sites with the valence of +2. Since the Cr valence was identical in the ZnCrTe and CrTe phases, any ferromagnetic property should arise from the +2 state of chromium. Therefore, these two phases might be the origin of the observed ferromagnetic behavior. Also, the spectra suggested that *d* shell electrons of Cr existed in the high spin state with four unpaired electrons per Cr^{2+}. The empty hybridizing *d* orbitals enhance the total spin of the system by the hybridization of 3*d* orbital from Cr and 5*p* orbitals from Te.[26–28]

3.4. AFM and MFM Analysis

Surface magnetic properties of the grown films were investigated by MFM analysis. Prior to measurements, the films were exposed to argon gas flow and, subsequently,

Table III. Relative atomic percentage of Zn, Te and Cr elements, as evaluated from the High-resolution surface XPS spectra of the $Zn_{1-x}Cr_xTe$ films with $x = 0.0$, $x = 0.05$, and $x = 0.15$

	Relative at.%		
$Zn_{1-x}Cr_xTe$	Zn	Te	Cr
$x = 0.0$	52.1	47.17	—
$x = 0.05$	45.0	50.03	4.97
$x = 0.15$	34.7	50.08	15.3

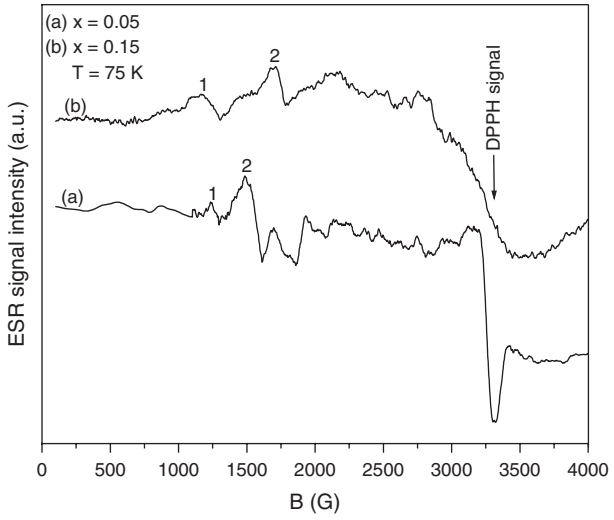

Fig. 6. X-band ESR spectra of $Zn_{1-x}Cr_xTe$ films with (a) $x = 0.05$ and (b) $x = 0.15$ grown onto GaAs (100) substrate recorded at 75 K.

the topographic observation was carried out by AFM. Figure 7(a) shows the topography of film with $x = 0.05$ in a region of 20×20 nm^2. The scale on the right indicates the root mean square roughness (RMS) of the area, with the color scale indicating the higher (white) and lower points (black) of the surface features. Figure 7(b) shows the corresponding MFM interactions observed in the same region. The circle indicates the area selected for the zoom. On the right, the color scale indicates the lower positions of repulsion with respect to the tip as dark regions, while the higher positions of attraction correspond to bright regions. Also the degree (deg) scale indicates the angular divergence of magnetic domains over the area of 20×20 nm^2. From the AFM study, the calculated average particle size was around 2 nm. The MFM mode allowed defining the interaction between domains in the same region of the film. The obtained image showed domains with weak interactions. Similarly, AFM and MFM images were recorded for the film with $x = 0.15$ as is shown in Figure 8 in the area of 500×500 nm^2. In this case, the average particle size was around 10 nm and the MFM image showed the domains as bright (attractive) and dark (repulsive) zones with respect to the tip.

3.4.1. Magnetic Domains

The region marked by the circles in Figures 7(b) and 8(b) were zoomed for further analyses in order to observe the domains in detail. High-resolution MFM images in 3D mode for the film with $x = 0.05$ are shown in Figures 9. The bright and dark contrast represents domains with positive (↑) and negative (↓) polarizations, where the domains form zigzag patterns with different orientation. This indicates that the interactions are related to anisotropic domain behavior in disordered distributions of

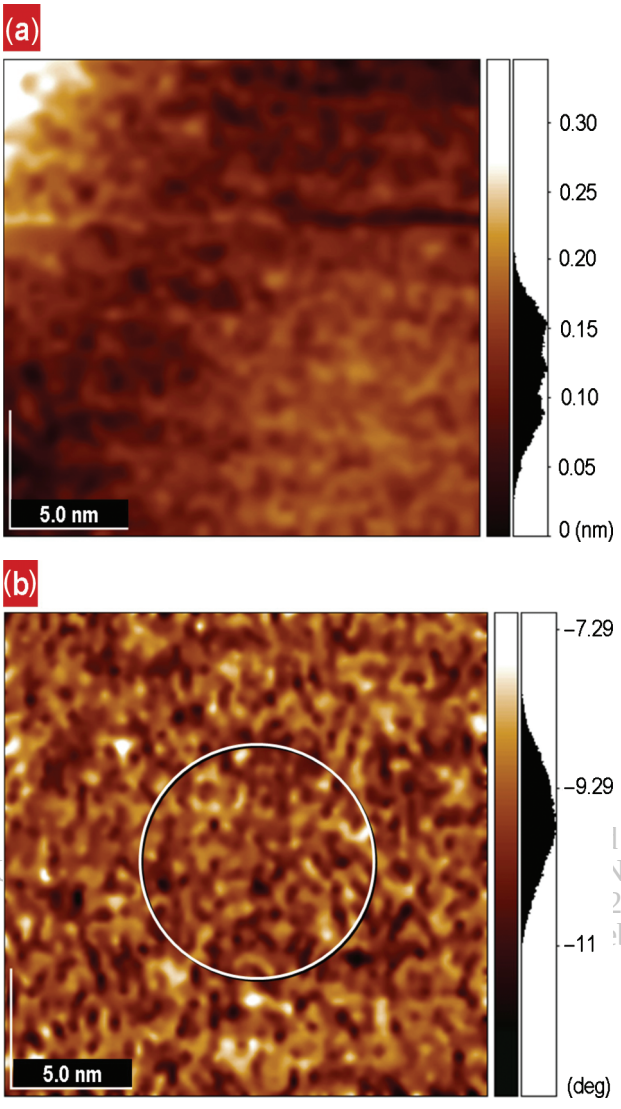

Fig. 7. 2D-view of AFM and MFM images of a $Zn_{1-x}Cr_xTe$ ($x = 0.05$) film grown onto a GaAs (100) substrate. (a) Nanoparticles in a scanned area of 20×20 nm^2. (b) Distribution of nanometer-sized magnetic domains in the same area. The marked region is zoomed for further analysis as in Figures 9(a)–(c).

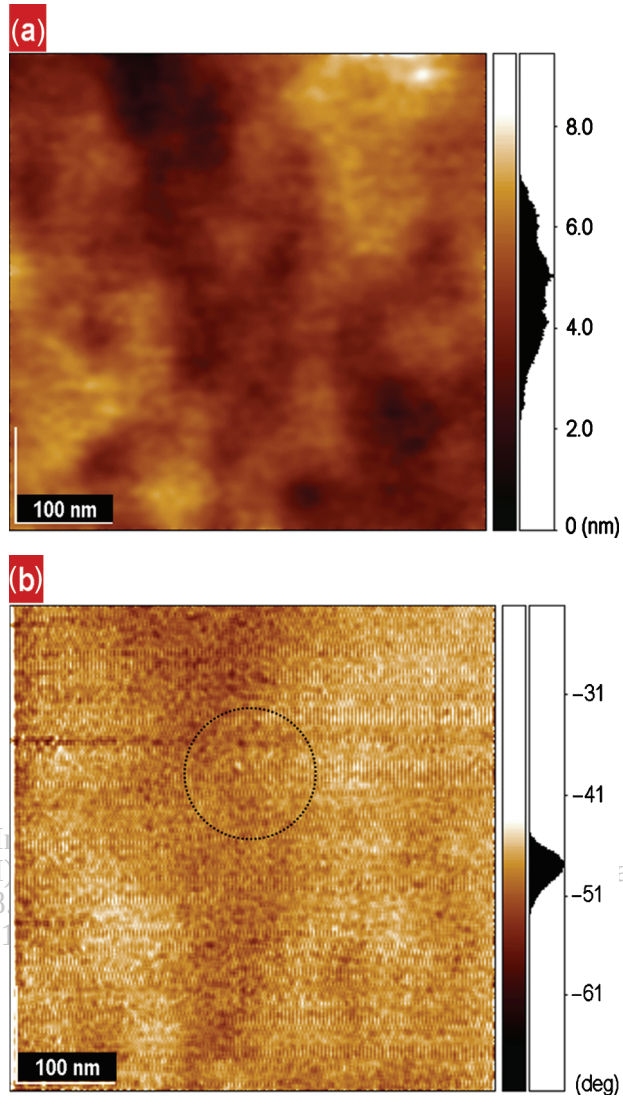

Fig. 8. 2D view of AFM and MFM images of a $Zn_{1-x}Cr_xTe$ ($x = 0.15$) film grown onto a GaAs (100) substrate. (a) Distribution of nanoparticles in the area of 500×500 nm^2; (b) Distribution of nanometer-sized magnetic domains in the same area. The marked region is zoomed for further analysis, as shown in Figure 10.

nanoparticles. Bottom of Figure 9(b) shows the cross sectional view of domains. The distribution of domains in the profile in Figure 9(c) indicates domains with an average size of 1 nm. The observed domains must have originated from cubic ZnCrTe phase and from the minute amorphous ZnCrTe/CrTe. In the case of films with ($x = 0.15$), the high-resolution images are illustrated in Figure 10. The domains followed preferential orientation with respect to the tip interaction and its behavior is associated with isotropic domain features. In this case, the average domain size was estimated to be about 2 nm. The observed domains must have originated from a major cubic ZnCrTe phase, a minor hexagonal ZnCrTe phase, and from the amorphous ZnCrTe/CrTe. Also, it was noted that the average domain size increased from 1 to 2 nm with increases in the Cr concentration. This supports the hypothesis that ferromagnetic order may be enhanced upon increasing the Cr content. The domains observed at room temperature indicate the existence of remanence magnetization over the film surface. The domains in the nanometer-size regime are due to the smaller particles in the films. The correlations between volume, surface defects and interaction of nanoparticles in the film result in local broken down exchange bonds and lead to nanometric domains.[29]

3.5. M–H Curves

The magnetic moment as a function of magnetic field on $Zn_{1-x}Cr_xTe$ ($x = 0.05$, 0.15) films was recorded at 300 K

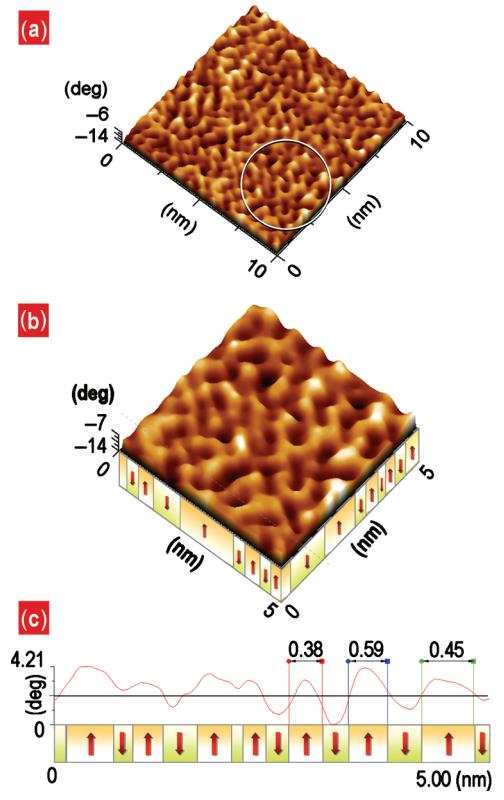

Fig. 9. (a) 3D view of domains in the 10×10 nm^2 region marked in Figure 7(b). (b) Zoom of the 5×5 nm^2 region marked in Figure 9(a), which shows bright and dark zones of anisotropic domains with opposite polarization. The bottom of the 3D image shows a cross-sectional view of the domains (c) Profile of domains in cross section of the image of (b). The average domain size over the film surface is 1 nm.

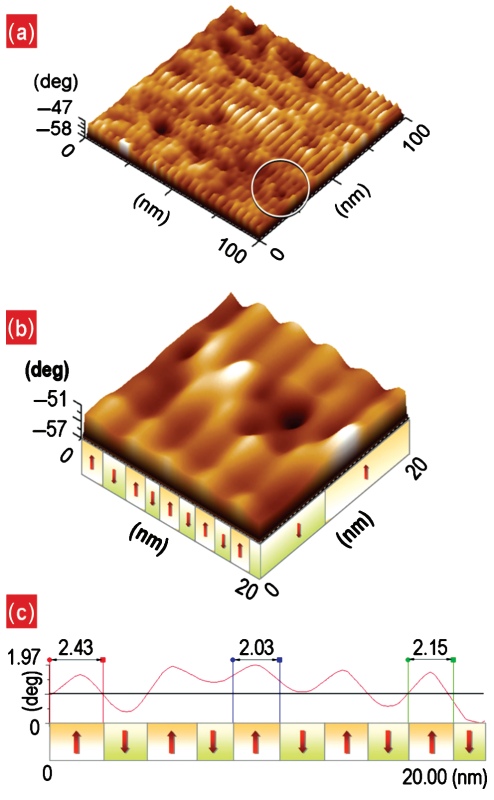

Fig. 10. 3D view of domains in the 100×100 nm^2 region marked in Figure 8(b). (b) Zoom of 20×20 nm^2 area selected in Figure 10(a), which clearly shows bright and dark regions of isotropic domains. (c) Cross-sectional view of the magnetic domain profile in image (b). The average domain size over the film surface was found to be about 2 nm.

and the obtained results are shown in Figure 11. In general, an obvious hysteresis loop was observed for film with $x = 0.05$ and a strong hysteresis loop was observed for film with $x = 0.15$. The coercive field (H_c) and remanence magnetic moment (M_r) were found to vary from 55 to 510 Oe and from 0.11×10^{-4} to 0.62×10^{-4} emu, respectively. It was clear that the ferromagnetic order in the prepared films increased with the Cr concentration. This is because of the increase of crystalline ZnCrTe phase in addition to the enhancement of the amorphous ZnCrTe/CrTe with increase in the Cr concentration. The joint increments of these ferromagnetic phases contribute for the observed strong hysteresis loop.

Also, an attempt was made to use Arrott plot analysis to estimate the values of the saturation magnetic moment or spontaneous magnetic moment (M_s) and of the Curie temperature (T_c). Arrott plots were realized by plotting the square of magnetic moment (M^2) versus H/M. In the Arrott plot, the intercept of a linear M^2 versus H/M plot, extrapolated to $H/M = 0$ from high magnetic fields, corresponds to the square of saturation or spontaneous magnetic moment (M_s^2). The saturation magnetic moment is zero when the straight line passes through the origin and the temperature at which this occurs is referred to as the Curie temperature.[30] The Arrott plots of the $Zn_{1-x}Cr_xTe$ ($x = 0.05$, 0.15) films are shown in the inset of M–H curves. In the case of film with $x = 0.05$, the plot clearly shows non-linearity. At the same time, the curvature does

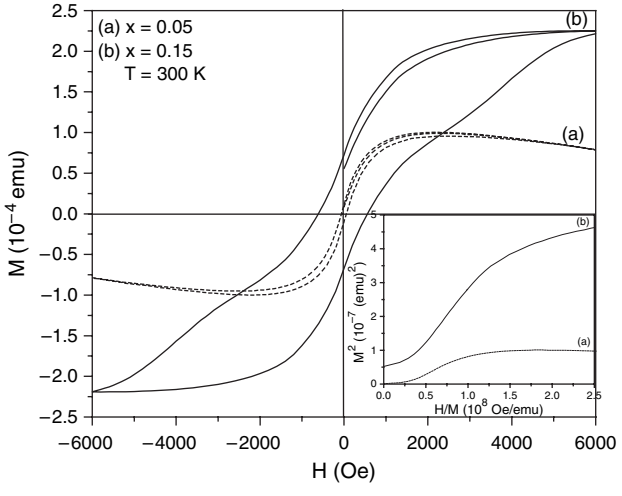

Fig. 11. Magnetic moment versus magnetic field (M–H) plots of $Zn_{1-x}Cr_xTe$ films with (a) $x = 0.05$ and (b) $x = 0.15$ grown on GaAs (100) substrate recorded at 300 K. Diamagnetic contribution from GaAs was subtracted. Inset shows the Arrott plot analysis of same M–H curves.

not pass through the origin even when the temperature reaches 300 K. This points out that the saturation magnetic moment did not drop to zero and, hence a weak ferromagnetic order persisted even when the field is removed. This fact indicated the presence of short-range ferromagnetic behavior for such low Cr concentration at 300 K. On the contrary, a deviation from non-linearity was clearly seen for film with $x = 0.15$. This suggested that at such higher Cr concentration, magnetic interactions tended to be long-range with improved spontaneous magnetic moment. In this case, the estimated value of the Curie temperature was much greater than 300 K.

4. CONCLUSIONS

ZnTe and Cr-doped ZnTe films were grown onto GaAs (100) by a thermal evaporation method. XRD patterns showed the presence of ZnCrTe phase with a minute amorphous ZnCrTe/CrTe, which increased slightly with increases in the Cr concentration. XPS analysis showed the presence of antiferromagnetic Cr_2O_3 and Cr phases. The valence state of Cr in ZnTe was determined to be +2 by using XPS and ESR spectra analysis, which indicated that any ferromagnetic behavior should originate from +2 state of Cr in both ZnCrTe and CrTe phases. MFM analysis showed the presence of magnetic domains whose average size was found to increase from 1 to 2 nm with increases in the Cr content. M versus H measurements revealed ferromagnetic hysteresis behavior at room temperature. By using Arrott analysis, the Curie temperature was estimated to be much greater than 300 K. It was concluded that, in addition to the presence of ZnCrTe phase, amorphous ZnCrTe/CrTe also contributed to the observed ferromagnetic behavior.

Acknowledgment: This work was supported by the World Class University Program (R33-2008-000-10147-0) from Ministry of Education, Science and Technology, Korea. The authors acknowledge C. Flores-Morales from the Instituto de Investigaciones en Materiales, IIM-UNAM for his technical support in AFM characterization.

References and Notes

1. S. Kuroda, N. Nishizawa, K. Takita, M. Mitome, Y. Bando, K. Osuch, and T. Dietl, *Nat. Mater.* 6, 440 (**2007**).
2. G. Krishnaiah, N. Madhusudhana Rao, B. K. Reddy, D. Raja Reddy, T. Mohan Babu, S. Sambasivam, and P. Sreedhara Reddy, *Phys. Lett. A* 372, 6429 (**2008**).
3. H. Ohno, A. Shen, F. Matsukura, A. Oiwa, A. Endo, S. Katsumoto, and Y. Iye, *App. Phys. Lett.* 69, 363 (**1996**).
4. H. Munekata, H. Ohno, R. R. Ruf, R. J. Gambino, and L. L. Chang, *J. Cryst. Growth* 111, 1011 (**1991**).
5. D. A. Allwood, G. Xiong, C. C. Faulkner, D. Atkinson, D. Petit, and R. P. Cowburn, *Science* 309, 1688 (**2005**).
6. I. Zutic, J. Fabian, and S. Das Sarma, *Rev. Mod. Phys.* 76, 323 (**2004**).
7. G. Prinz, *Science* 282, 1660 (**1998**).
8. I. A. Buyanova, G. Yu Rudko, W. M. Chen, A. A. Toropov, S. V. Sorokin, S. V. Ivanov, and P. S. Kop'ev, *Appl. Phys. Lett.* 82, 1700 (**2003**).
9. D. Ferrand, J. Cibert, A. Wasiela, C. Bourggnon, S. Tatarecko, G. Fishman, T. Andrearczyk, J. Jaroszynski, S. Jolesnik, T. Dietl, B. Barbara, and D. Dufeu, *Phys. Rev. B* 63, 85201 (**2001**).
10. S. E. Park, H. J. Lee, Y. C. Cho, and S. Y. Jeong, *App. Phys. Lett.* 80, 4187 (**2002**).
11. T. Fukushima, K. Sato, H. Katayama-Yoshida, and P. H. Dederichs, *Jpn. J. Appl. Phys.* 43, L1416 (**2004**).
12. X. G. Guo, J. C. Cao, X. S. Chen, and W. Lu, *Solid State Commun.* 138, 275 (**2006**).
13. H. Saito, V. Zayets, S. Yamagata, and K. Ando, *Phys. Rev. B* 66, 081201 (**2002**).
14. H. Saito, V. Zayets, S. Yamagata, and K. Ando, *Phys. Rev. Lett.* 90, 207202 (**2003**).
15. H. Saito, S. Yamagata, and K. Ando, *J. Appl. Phys.* 95, 7175 (**2004**).
16. N. Ozaki, N. Nishizawa, S. Kuroda, and K. Takita, *J. Phys. Condens. Matter* 16, 5773 (**2004**).
17. D. Soundararajan, D. Mangalaraj, D. Nataraj, L. Dorosinskii, J. Santoyo-Salazar, H. C. Jeon, and T. W. Kang, *Appl. Surf. Sci.* 255, 7517 (**2009**).
18. D. Soundararajan, D. Mangalaraj, D. Nataraj, L. Dorosinskii, J. Santoyo-Salazar, and M. J. Riley, *J. Magn. Magn. Mats.* 321, 4108 (**2009**).
19. JCPDS, X-ray powder diffraction file, Joint Committee for Powder Diffraction Standards (Card numbers: 80-0022 & 80-0009).
20. S. Kuroda, N. Ozaki, N. Nishizawa, T. Kumekawa, S. Marcet, and K. Takita, *Sci. & Tech. of Advan. Mats.* 6, 558 (**2005**).
21. C. D. Wagner, W. M. Riggs, L. E. Davis, J. F. Moulder, and C. E. Muielenberg, Handbook of X-Ray Photoelectron Spectroscopy, Physical Electronics Industries, Eden Prairie, MN (**1976**).
22. C. Xu, M. Hassel, H. Kuhlenbeck, and H.-J. Freund, *Surf. Sci.* 258, 23 (**1991**).
23. X.-Y. Li, E. Akiyama, H. Habazaki, A. Kawashima, K. Asami, and K. Hashimoto, *Corros. Sci.* 39, 1365 (**1997**).
24. D. Soundararajan, D. Mangalaraj, D. Nataraj, L. Dorosinskii, and J. Santoyo-Salazar, *J. Phys.: Conf. Ser.* 153, 012048 (**2009**).
25. S. N. Mishra and S. K. Srivastava, *J. Phys.: Condens. Matter* 20, 285204 (**2008**).
26. J. Blinowski, T. Dietl, and P. Kacman, *Acta Phys. Pol. A* 82, 641 (**1992**).
27. J. Blinowski and P. Kacman, *Phys. Rev. B* 46, 12298 (**1992**).
28. W. Mac, N. T. Khoi, A. Twardowski, and J. A. Gaj, *Phys. Rev. Lett.* 71, 2327 (**1993**).
29. G. Salazar-Alvarez, J. Qin, V. Šepelák, I. Bergmann, M. Vasilakaki, K. N. Trohidou, J. D. Ardisson, W. A. A. Macedo, M. Mikhaylova, M. Muhammed, M. D. Baró, and J. Nogués, *J. Am. Chem. Soc.* 130, 13237 (**2008**).
30. A. Arrott, *Phys. Rev.* 108, 1394 (**1957**).

Received: 18 June 2009. Accepted: 28 July 2010.